Shell-filling effects and Coulomb degeneracy in planar quantum-dot structures

Satyadev Nagaraja, Philippe Matagne, Voon-Yew Thean, and Jean-Pierre Leburton
Beckman Institute for Advanced Science and Technology, University of Illinois at Urbana-Champaign, Urbana, Illinois 61801

Yong-Hoon Kim and Richard M. Martin
Department of Physics, University of Illinois at Urbana-Champaign, Urbana, Illinois 61801

(Received 17 March 1997; revised manuscript received 7 July 1997)

We investigate the influence of electron-electron interactions on the electronic properties of quantum dots in a regime where the energy-level separation is comparable to or larger than the Coulomb charging energy at low temperature ($e^2/2C \gg k_BT$). A self-consistent three-dimensional solution of Schrödinger and Poisson equation within the local-density approximation is implemented to study the formation of shell structure in highly symmetric quantum dots which is in good agreement with recent experimental results [Tarucha *et al.*, Phys. Rev. Lett. **77**, 3613 (1996)] For asymmetric quantum dots, we show that the shell structure disappears, and features due to electron-electron interaction lead to the accidental formation of an isolated electron shell called ''Coulomb degeneracy'' in the energy spectrum. [S0163-1829(97)02648-9]

I. INTRODUCTION

Quasi-zero-dimensional systems, such as quantum dots, have been the subject of intense research in recent years,[1,2] owing to the development of sophisticated patterning and nanofabrication techniques that make possible the realization of systems of very small and precise dimensions with characteristic sizes comparable to the de Broglie wavelength of carriers.[3–6] Because the capacitance C associated with such systems is extremely small ($\simeq 10^{-16}$ F), the single-electron charging energy given by $e^2/2C$ could be of the order of a few meV, which at low enough temperature, i.e., for $e^2/2C \gg k_BT$, leads to the observation of ''Coulomb blockade'' and single-electron tunneling.[7–9] The distribution of electron states in the dot has an important bearing on its electrostatic and transport properties. In metallic dots, because of the large electron effective mass, single-particle states are barely resolved so that the energy spectrum is a quasicontinuum, making the single-electron charging energy entirely due to the Coulomb repulsion from the electrons in the dot–this is the Coulomb blockade regime described by the orthodox theory.[10] On the other hand, semiconductor quantum dots, which can be grown with precise dimensions of a few hundred angstroms, have usually lower electron effective masses that result in well-quantized energies whose separation ΔE is comparable to the Coulomb charging energy $e^2/2C$. The level separation, in addition to the Coulomb repulsion, makes an additional contribution to the single-electron charging energy of the dot—this is the quantized regime. In this regime, owing to the three-dimensional (3D) quantum confinement of electrons, quantum dots (QD's) may be considered as analogs of natural atoms with two fundamental differences: in atoms, the Coulomb field is spherical and quantized in units of the elementary charge because of the discreteness of nuclear charge, while in QD's the confining potential may have arbitrary geometry and is continuous in terms of the elementary charge. However, in highly symmetric QD's, the quantized energies may exhibit orbital degeneracies and form shells when occupied by electrons, as in atoms.[11] The filling of successive shells in QD's depends on factors such as electron-electron interaction and the electron spin.[7]

In this work, we investigate the influence of the confining potential and the role of electron-electron interaction in the formation of shell structure in planar quantum dots (PQD's) achieved by confining a two-dimensional electron gas (2DEG) by means of patterned gates.[12,13] We consider two PQD configurations: a square-gate dot which when empty has a nearly circularly symmetric confining potential, and a quad-gate dot which has a rectangular symmetry. For this purpose, we solve self-consistently the 3D Schrödinger and Poisson equations. Our model generalizes previous approaches which tackle similar problems in recent years by either excluding exchange-correlation effects,[14] or neglecting quantization effects normal to the heterointerface,[15] or assuming the adiabatic approximation where the separation between the quantized levels in the dot, ΔE, is comparable to k_BT,[8] or finally by considering dots with large number N ($\geqslant 70$) of electrons.[9] We consider PQD's with $\Delta E \simeq e^2/2C \gg k_BT$ and small N ($\leqslant 20$) and use an efficient technique, called the iterative extraction orthogonalization method (IEOM), to solve the 3D Schrödinger equation.[8] The ability of this method to generate an arbitrarily small number of eigenstates makes it suitable for the simulation of nanostructures exhibiting a small number of occupied states. We solve the single-particle Schrödinger equation, and include many-body exchange-correlation effects under the local-density approximation (LDA). We neglect Coulombic fluctuations due to ionized impurities in the dot, and assume abrupt interfaces at the GaAs-$Al_{0.3}Ga_{0.7}As$ boundary.

In Sec. II we describe the two dot structures. In Sec. III we discuss the computational model and briefly review the IEOM method for solving Schrödinger equation. We also discuss the method of determining the equilibrium electron population of the dot from an evaluation of the Gibbs free energy.[1,2] In Sec. IV we discuss the boundary conditions imposed on the potential and the wave functions in the various regions of the device. We present our results in Sec. V,

 © 1997 The American Physical Society

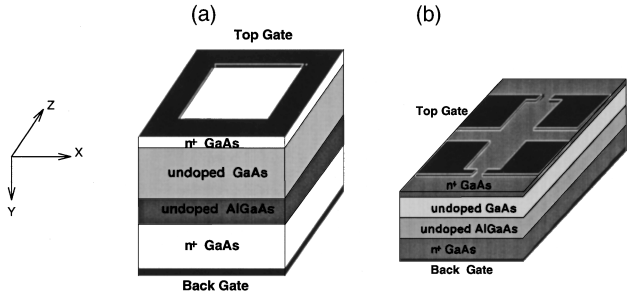

FIG. 1. Schematic representation of (a) a square and (b) a quad-gate quantum-dot device with layer structure.

where for the square-gate dot we obtain deep physical insights in the formation of shell structure in agreement with the recent experimental findings of Tarucha *et al.*[7] Furthermore, we discuss the variations in the shell structure introduced by an asymmetric confining potential, in a rectangular quad-gate device. We show that the electron-electron interaction leads to an effect called ''Coulomb degeneracy'' that results from a collapse of states on the Fermi level due to electron-electron interaction. We calculate the addition energies and the gate-dot capacitance for the two devices. From these findings, we draw conclusions in Sec. VI.

II. DOT STRUCTURES

The devices investigated here are shown in Fig. 1. They consist of an inverted GaAs/$Al_{0.3}Ga_{0.7}As$ heterostructure that confines the electrons to a 2D gas at the interface. In our model, the simulated structure consists of a 22.5-nm layer of undoped $Al_{0.3}Ga_{0.7}As$ followed by a 125-nm layer of undoped GaAs and finally an 18-nm GaAs cap layer. The cap layer is uniformly doped to $5\times10^{18}\ \mathrm{cm}^{-3}$ so that the conduction-band edge is just above the Fermi level at the GaAs-cap-layer–undoped GaAs boundary. The inverted heterostructure is grown on a GaAs substrate and charge control is achieved by varying the voltage on the back gate V_{back}. We assume a negligible voltage drop across the substrate; hence we apply V_{back} directly to the bottom of the $Al_{0.3}Ga_{0.7}As$ layer. The first quantum dot shown in Fig. 1(a) has a $240\times240\ \mathrm{nm}^2$ square open area at the top bordered by a 65-nm-thick gate. This device is only of academic importance, since the barriers are too thick to allow electron injection through tunneling. However, it is well suited to study properties such as electronic spectrum and dot filling. The quad-gate device has four gate pads with 45-nm stubs protruding into the channel; the dimensions of the open area on the top are $230\times408\ \mathrm{nm}^2$. Electron charging of the dot is possible through tunnel injection from the adjacent two-dimensional regions through the 70-nm opening between the stubs along the x direction. The separation between the pads along the (longer) z direction is 90 nm.

III. COMPUTATIONAL MODEL

In order to study the electronic properties of the quantum dot, the Schrödinger equation is solved in the central 0D region. The Hamiltonian reads

$$\hat{H}=-\frac{\hbar^2}{2}\nabla\left[\frac{1}{m^*(\mathbf{r})}\nabla\right]+E_c(\mathbf{r})+\mu_{\mathrm{xc}}(n), \tag{1}$$

where $m^*(\mathbf{r})$ is the position-dependent effective mass of the electron in the different materials, $E_c(\mathbf{r})=\phi(\mathbf{r})+\Delta E_{\mathrm{os}}$ is the conduction-band edge, where $\phi(\mathbf{r})$ is the electrostatic potential, ΔE_{os} is the conduction-band offset, and $\mu_{\mathrm{xc}}[n]$ is the exchange and correlation potential as parametrized by Ceperley and Alder[16] (see the Appendix).

The 3D Poisson equation for the electrostatic potential $\phi(\mathbf{r})$ reads

$$\nabla[\epsilon(\mathbf{r})\nabla\phi(\mathbf{r})]=-\rho(\mathbf{r}), \tag{2}$$

where the charge density $\rho(\mathbf{r})$ is given by $e[p(\mathbf{r})-n(\mathbf{r})+N_D^+(\mathbf{r})-N_A^-(\mathbf{r})]$. Here $\epsilon(\mathbf{r})$ is the permittivity of the material and is a function of y only throughout this work, $p(\mathbf{r})$ is the hole concentration, $n(\mathbf{r})$ is the electron concentration, and $N_D^+(\mathbf{r})$ and $N_A^+(\mathbf{r})$ are the ionized donor and acceptor concentrations, respectively. Electron wave functions obtained from the Schrödinger equation are used to calculate $n(\mathbf{r})$ inside the dot, and a classical charge density obeying Thomas-Fermi distributions are used in the regions outside the dot. In the dot

$$n(\mathbf{r})=\sum_i f(E_i)|\psi_i(r)|^2, \tag{3}$$

where $f(E_i)$ is the occupation probability of the level E_i. If the dot is in strong diffusive contact with the reservoirs, $f(E_i)$ is the Fermi-Dirac distribution function. Otherwise, $f(E_i)$ is evaluated from the grand canonical ensemble by imposing the condition on Gibbs distribution that only an integer number of electrons N can occupy the dot.[1,10]

We map the device onto a three-dimensional grid made of rectangular parallelepipeds; with $36\times33\times36$ grid points (for the square-gate device) along $x\times y\times z$. We solve Poisson's equation using an iterative Newton's technique, in which the new solution for the potential ϕ_{new} is combined with the solution ϕ_{old} obtained from the previous iteration by using a simple relaxation technique to get the potential $\phi=(1-\alpha)\phi_{\mathrm{old}}+\alpha\phi_{\mathrm{new}}$. The relaxation parameter α is usually between 0.95 and 0.99. In solving the Schrödinger equation we use the IEOM developed by Kosloff and Tal-Ezer.[17] This method is fast and efficient, compared to conventional eigenvalue solvers, when solving for a few eigenvalues (e.g., 20), and is consequently suitable for quantum dot calculations.[8]

The basic idea behind the method is the construction of a functional of the Hamiltonian $F(\hat{H})$ that extracts the lowest eigenvalue state (the ground state) from a trial wave function, $|\alpha\rangle$, consisting of a mixture of basis states $|m\rangle$, i.e.,

$$F(\hat{H})|\alpha\rangle=\sum_m |m\rangle F(E_m)\langle m|\alpha\rangle=|0\rangle F(E_0)\langle 0|\alpha\rangle + \sum_{m=1} |m\rangle F(E_m)\langle m|\alpha\rangle. \tag{4}$$

If $F(E_m)$ decreases with increasing E_m, the term containing the lowest state dominates over the second term. Hence, when $F(\hat{H})$ is successively applied to the updated wave function, the higher-order contributions in $m\geqslant1$ eigenstates

become negligible and the ground state emerges progressively. The M higher excited states are obtained by applying $F(\hat{H})$ to M different guess states and by orthogonalizing them with a Gram-Schmidt technique after each iteration. The chosen functional, however, must have a well-behaved Taylor expansion; an exponential form $\exp(-\gamma\hat{H})$ satisfies this criterion.

In practice, Schrödinger and Poisson equations are solved until self-consistency is obtained—when the difference between the calculated eigenenergies, in successive iterations, is smaller than 10^{-6} eV and the residue in the Poisson equation is 10^5 V cm^{-2} per grid point, which determines the potential to an accuracy of less than 10^{-6} eV. It should be pointed out that the self-consistency of the Poisson-Schrödinger equations does not guarantee that the number of electrons N in the dot is an integer. From a general standpoint N is determined by minimizing the Gibbs free energy $F(N)$ with respect to N for each gate bias configuration. $F(N)=-k_BT\ln Z$ is derived from the partition function Z for the grand canonical ensemble,[8] which reads

$$Z(N)=\sum_{\{n_i\}} \exp\left[\frac{\sum_{i=1}^{\infty} n_iE_i-E_H(N)-\mu N}{k_BT}\right], \tag{5}$$

where the summation is over all possible electron configurations at constant $N=\Sigma_i n_i$ and n_i is either 0, 1, 2 reflecting the occupancy of the level E_i. Double counting of the Coulombic interaction is avoided by subtracting the Hartree energy for N electrons,

$$E_H(N)=\frac{1}{2}\int\int \frac{\rho(\vec{r})\rho(\vec{r}')}{|\vec{r}-\vec{r}'|}\,d\vec{r}\,d\vec{r}', \tag{6}$$

in the evaluation of Z. The computation of $F(N)$ requires the evaluation of Z by considering all configurations with the occupation of levels positioned several k_BT from the Fermi level E_F. This approach is computationally expensive for level separation $\Delta E \gg k_BT$, as in the present case (i.e., $\Delta E \simeq 100\,k_BT$). Therefore, we determine N by minimizing $F(N)$ only when a level is close ($\simeq k_BT$) to E_F. When the lowest unoccupied level is far away (i.e., several k_BT) from the Fermi level, N is simply twice the number of eigenlevels below E_F.

IV. BOUNDARY CONDITIONS

For computation purposes, the device is divided into regions of various dimensionalities characterizing the degrees of freedom of electrons in their respective regions. We assume that the wave functions vanish at the boundary surfaces of each of the regions. This condition has to be used with caution in the quad-gate device, where the higher states extend deeper into the barriers under the stubs. However, in a small-N problem such as the present one, the states of interest are well confined and do vanish at the boundary surface of the dot.

The potential is determined by Dirichlet boundary conditions on the exposed surfaces at the top and bottom of the structure where the Fermi-level pinning modifies the Schottky barrier heights by ϕ_s-V_G, where V_G is the gate bias. In the lateral x-z directions von Neumann conditions, where the electric field vanishes at a distance far enough from the dot, are assumed. Hence, solving rigorously the Poisson Equation (2) by imposing the equipotential boundary conditions at the gates eliminates the need to include explicitly the effect of the image charge as a correction to the electron-electron interaction.

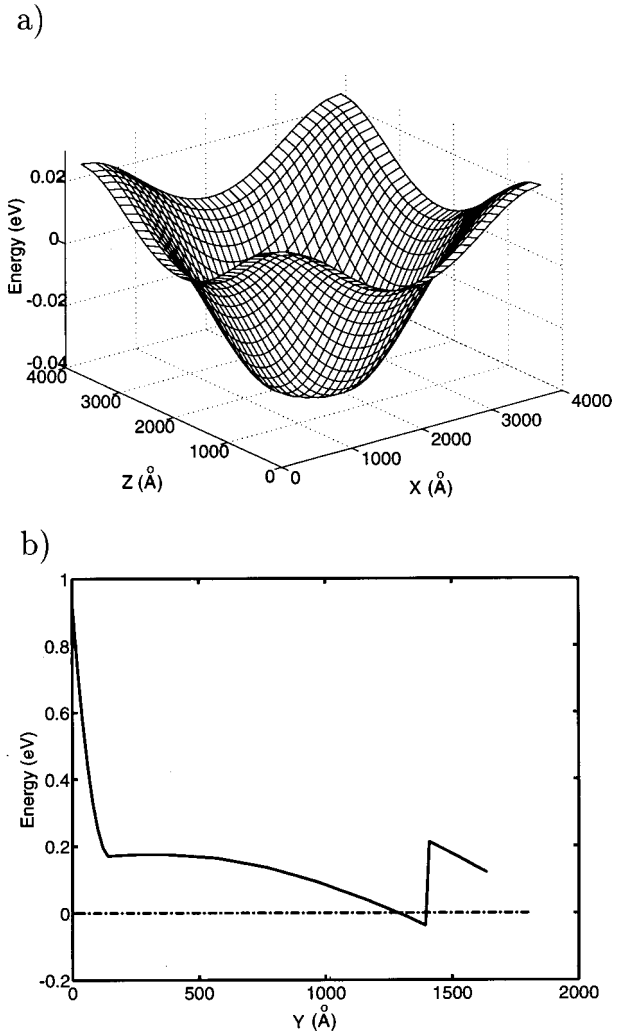

FIG. 2. Conduction-band edge of the square-gate dot for $V_{\text{back}}=0.9735$ V at $T=0.25$ K (a) on the x-z plane (b) along the vertical y direction through the center of the dot.

V. RESULTS

Figure 2(a) shows the conduction-band edge at the GaAs-$Al_{0.3}Ga_{0.7}As$ interface for the square-gate structure in the lateral x-z plane, and Fig. 2(b) shows the variation of the conduction-band edge perpendicular (along the y direction) to the heterojunction, for an empty dot at $T=0.25$ K. The confinement in the x-z plane is parabolic with a barrier height of about 50 meV over a distance of 1800 Å. In the y direction, the confinement is defined by the conduction-band offset of 255 meV between GaAs and $Al_{0.3}Ga_{0.7}As$ and a large electrostatic y field, $F_y\simeq 35$ kV/cm, in GaAs. Consequently, the energy levels are spaced 30–40 meV apart along the y direction, and 1 meV apart in the x-z plane. Furthermore, the parabolic confinement in the lateral x-z plane induces a quadratic variation of the conduction-band edge

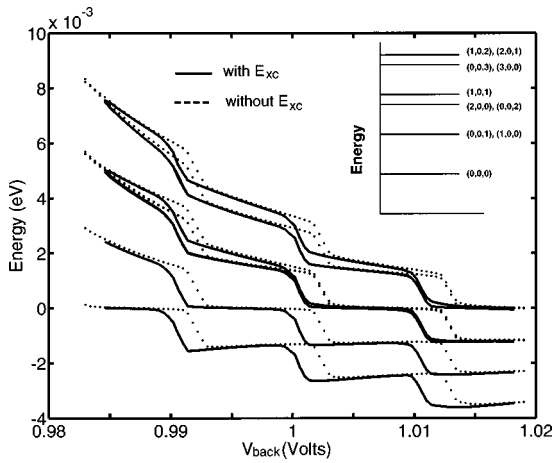

FIG. 3. Variation of the single-particle energy levels with V_{back} for the square-gate dot. The zero of the energy scale is the Fermi level. The effect of the exchange-correlation energy E_{ca} is discernable as a shift that increases with V_{back} in the energy levels to lower voltages. The inset shows the schematic of the energy spectrum for the empty $(N=0)$ dot with level ordering.

along the y direction (150 Å$\leqslant y \leqslant$1100 Å) in the charge-free region in GaAs [Fig. 2(b)], as opposed to a linear variation that would be expected if the system were translationally invariant in the x-z plane.

The inset in Fig. 3 shows the energy spectrum of the square-gate dot at $N=0$ with the corresponding degenerate states for each level. We label states as (n_x, n_y, n_z), where n_x, n_y, and n_z are the nodes along the x, y, and z directions, respectively. n_y is zero throughout this work, since the large spacing between states along the y direction precludes states other than the ground state from being occupied. Because of the parabolic shape of the external potential (arising from the gates and the ions) the six lowest localized wave functions achieve the 2D harmonic-oscillator symmetry in the empty dot, i.e., when the many-body effects are neglected.[14] The (0,0,0) state is the ground state with spin degeneracy only; consequently it can be occupied by two electrons. The (1,0,0) and (0,0,1) states are degenerate since they are identical except for a 90° symmetry rotation and accommodate four electrons. The (2,0,0) and (0,0,2) states are degenerate and constitute the third level accommodating six electrons. As with the (1,0,0) and (0,0,1) states, the (2,0,0) and (0,0,2) states are identical except for a 90° symmetry rotation. The (1,0,1) being of a different symmetry is slightly split (and higher in energy) from the (0,0,2) and (2,0,0) states. A similar situation arises in the fifth level which accommodates eight electrons: the (0,0,3) and the (3,0,0) differ by a 90° symmetry rotation; so also the (1,0,2) and the (2,0,1) states; the (1,0,2) and the (2,0,1) states are slightly higher in energy than (0,0,3) and the (3,0,0)-states.

The variation of the single-particle energy levels as a function of the back-gate voltage V_{back}, for the square-gate device, is shown in Fig. 3. The lowest ten states in the figure form the first four levels with degeneracies 1, 2, 3, and 4 with filling of two, four, six, and eight electrons, respectively. Also shown in the figure is the effect of exchange-correlation energy E_{XC} on the single-particle levels. The levels are seen to be shifted to the left (shown in solid lines in Fig. 3), i.e., to lower values of V_{back}, upon the inclusion of E_{XC}, due to the attractive nature of E_{XC}. It is to be noted that this shift is not constant but increases with the number of electrons in the dot, as is expected.

It is seen in Fig. 3 that at low values of V_{back}, i.e., $\leqslant$0.985 V, the energy levels are equally spaced about 3 meV apart. At $V_{\text{back}}=0.980$ V, the lowest energy level E_0 is about 2 meV, i.e., about 100 k_BT above the Fermi level and is not occupied. As V_{back} increases, E_0 lowers towards the Fermi level, and at $V_{\text{back}}\cong 0.985$ V, is occupied with the first electron. At this stage, E_0 does not continue to lower with increasing V_{back}, but sticks to the Fermi level, as dropping below the Fermi level would fully occupy the level with two electrons. This cannot happen until V_{back} is large enough to overcome the Coulomb repulsion due to the first electron already in the dot, which occurs at $V_{\text{back}}=0.9874$ V for which E_0 is fully occupied and falls below the Fermi level. It is seen that in the V_{back} interval required for charging E_0, the upper levels follow more or less the behavior of E_0. A further increase in V_{back} causes an abrupt lowering of E_0 and the upper levels, as the first shell is completely filled and the dot prepares to take on the third electron. The energy levels continue to decrease with increasing V_{back} until E_1 is partially occupied with one electron, i.e., $N=3$ at $V_{\text{back}}\cong 0.993$ V. Notice that the increase in V_{back} required for the $N=2$ to $N=3$ transition, i.e., $\Delta V=5.6$ mV, is greater than $\Delta V=2.4$ mV required for the $N=1$ to $N=2$ transition because, aside from overcoming the Coulomb repulsion due to two electrons in the dot, the lowering of the level E_1 towards the Fermi level requires additional energy. Similar to the behavior of E_0, E_1 sticks to the Fermi level until V_{back} is large enough to fully charge the shell with four electrons which occurs at $V_{\text{back}}=0.9982$ V on the figure. Further increase in V_{back} causes an abrupt lowering of E_1, similar to the behavior of E_0 at $V_{\text{back}}=0.9874$ V. The charging of level E_2 is similar to E_0 and E_1 but E_2 remains on the Fermi level over a longer voltage range, i.e., $\Delta V=9.6$ mV ($1.0026 \leqslant V_{\text{back}} \leqslant 1.0122$ V), since E_2 can accommodate six electrons, thereby requiring a greater increment in V_{back} to fully charge the shell.

Three observations can be made from the data provided in Fig. 3: Firstly, there is an abrupt lowering of energy levels at those values of V_{back} corresponding to the filling of a shell, which lead to a steplike behavior of the energy spectrum. This steplike behavior is similar to the results obtained by Stopa[18] with a different approach for analyzing the charging properties of large QD's characterized by a large number of electrons ($N\geqslant 70$). It is however different from the results of Jovanovic and Leburton[8] that show a relatively smooth spectra in large dots in the regime where $e^2/2C \gg \Delta E$ and $k_BT \gg \Delta E$. Secondly, the width of each step is proportional to the energy required to charge completely each of the constituent degenerate states of a level, and hence is proportional to the degeneracy of the level. Lastly, the energy levels get closer as V_{back} increases which is due to a decrease in the depth of the confining potential caused by the Hartree energy, accompanied by an increase in the dot area.

It is worthwhile mentioning that the sticking of a level to the Fermi level is a direct consequence of the LDA which cannot resolve individual spins. Hence, in our model it is not possible to determine the order in which the constituent degenerate states of a level are occupied by single spin elec-

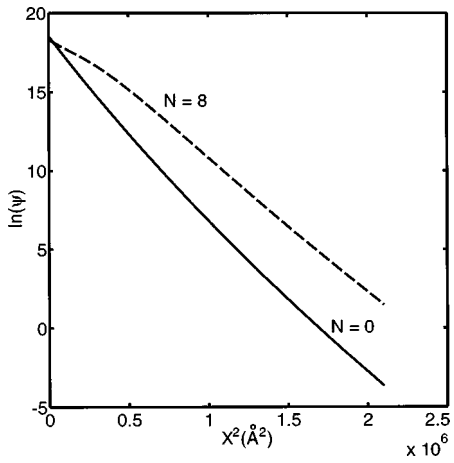

FIG. 4. Variation of $\ln \psi_{000}(x;z,y)$ with x^2 ($x=0$ is the center of the dot) for $N=0$ (solid line) and $N=8$ (dot-dashed line).

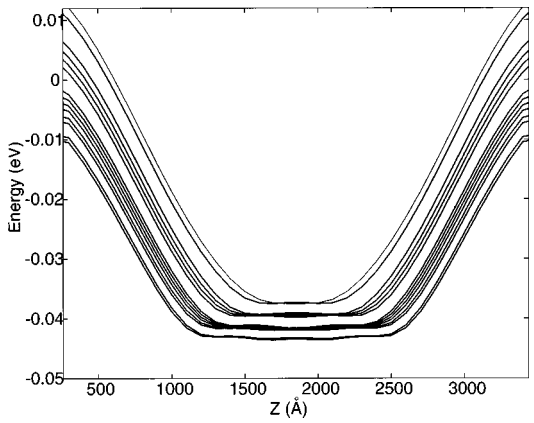

FIG. 5. Conduction-band edge along the x direction in the center of the square-gate dot, for N ranging from 1 to 14. The shell structure of the dot energies is manifested in the bunching of the conduction-band bottom for various N.

trons. Consequently, a level is constrained to remain at the Fermi level until V_{back} is large enough to fully charge this level. This constraint is removed if the model assigns individual levels to each spin state, like in the local spin-density approximation,[19] for instance, since it would then be possible to determine exactly the occupancy of the individual spin states at their crossings with the Fermi level as they are lowered with increasing V_{back}. However, this investigation is beyond the scope of this paper and will be addressed in a future work.[20]

Another feature evident from Fig. 3 is the splitting of the (1,0,1) and (2,0,0)-(0,0,2) states in the third level for $0.985 \leqslant V_{\text{back}} \leqslant 1.00$ V and the (2,0,1)-(1,0,2) and (0,0,3)-(3,0,0) states in the fourth level for $0.985 \leqslant V_{\text{back}} \leqslant 1.01$ V. This partial lifting of degeneracy in the third and the fourth levels is a consequence of the anhamonicity in the confining potential introduced by the many-body effects in the dot. The circular symmetry of the potential is lost, thereby increasing the separation between the (1,0,1) state and the (2,0,0)-(0,0,2) pair states (which continue to be degenerate as they are identical, but for a 90° symmetry rotation) in the third level, and between the (3,0,0)-(0,0,3) pair and the (2,0,1)-(1,0,2) pair states in the fourth level. Notice that at $V_{\text{back}} \cong 1.01$ V the split states merge again because of the Coulomb repulsion during the charging of the (2,0,0)-(0,0,2) levels which prevents the (1,0,1) state from crossing the former pair states.

Figure 4 shows, on a semilogarithmic scale, the profile of $\psi_{000}(x;y,z)$ at the heterointerface as a function of x^2. The variation of $\ln[\psi_{000}(x;y,z)]$ with x^2 is linear over 500 Å from the center of the dot for $N=0$, unlike that for $N=8$ which is only piecewise linear over that range. The linear variation of $\ln[\psi_{000}(x;y,z)]$ is to be expected for the ground-state wave function, which in a harmonic potential varies as $e^{-\alpha x^2}$. The piecewise linear behavior of $\ln[\psi_{000}(x;y,z)]$ is further evidence for the distortion in the confining potential due to electron-electron interaction.

Figure 5 shows the potential profile along the x direction for increasing values of V_{back}. The zero of the energy scale is the Fermi level. Each of the curves corresponds to the potential calculated just after the addition of an electron to the dot, starting from $N=1$ (the highest curve) to $N=14$ (the lowest curve). It is seen that the potential energy drops, as expected, when V_{back} is increased to charge the dot with electrons. The potential also flattens, as mentioned before, with increasing N reflecting the Coulomb interaction. The remarkable feature here is the grouping of the potential curves in a series of tight potential ''bunches'' that are indicative of the shell structure in the dot. A closer examination reveals the ''bunching'' of the first two curves for the first shell, the next four curves corresponding to the filling of the second shell ($N=6$) and the next six curves corresponding to the filling of the third shell ($N=12$), and so on. This is the clearest manifestation of ''shell filling.''

Figure 6 shows the Coulomb staircase as a function of V_{back} for the first eighteen electrons in the square dot. Each step indicates the increment in V_{back} (and hence the energy) required to add an electron to the dot. Unlike the conventional Coulomb blockade effects, the steps of the staircase are of unequal width with wide steps corresponding to the complete filling of a shell. Indeed the steps are grouped according to the degenerate single-particle orbitals with wide steps indicating a jump to the next orbital, starting with two electrons, then four, six, etc. Also noticeable is the general trend for the steps to become narrower with high V_{back}, which results from an increase in the dot capacitance due to an expansion of the dot, as well as a decrease in the energy-level spacings due to decreased confinement.

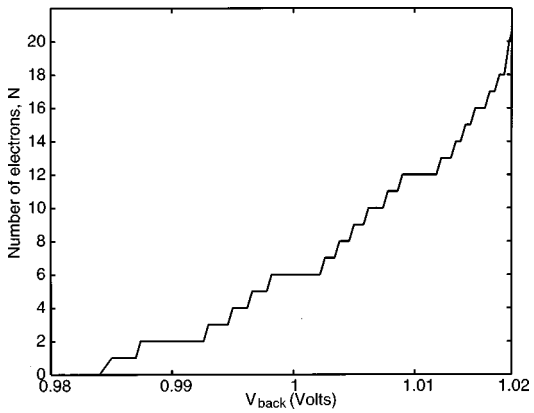

FIG. 6. Coulomb staircase for the square-gate quantum dot; the top gates are fixed at -1.9 V.

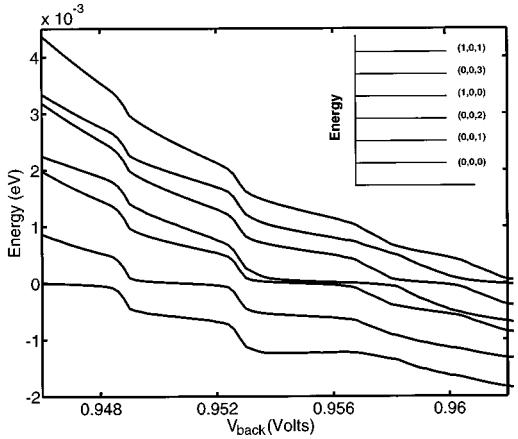

FIG. 7. Variation of the single-particle energy levels with V_{back} for the quad-gate dot. The zero of the energy scale corresponds to the Fermi level. The inset shows the schematic of the energy spectrum of the empty ($N=0$) dot with level ordering.

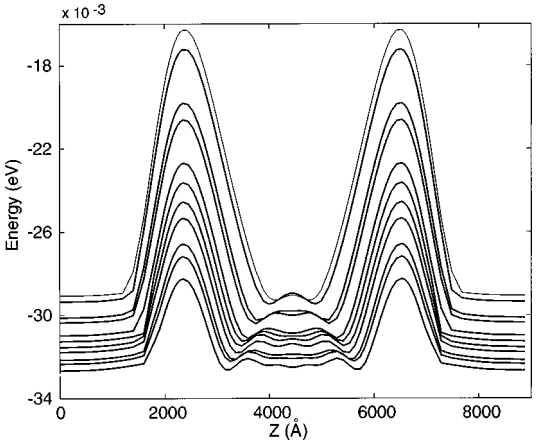

FIG. 8. Conduction-band edge, along the z direction in the center of the quad-gate dot for N ranging from 1 to 11 showing the bunching of the conduction band edge for the fifth, sixth, seventh, and eighth electron under Coulomb degeneracy.

In contrast to the square-gate dot, the quad-gate dot depicted in Fig. 1(b) has no energy level degeneracies, and hence no shell structure, due to its rectangular geometry as shown schematically in the inset of Fig. 7 with the ordering of the energy levels.

Figure 7 shows the variation of the single-particle energy spectrum with V_{back} for the quad-gate dot. The variation is qualitatively similar to the square-gate device except that each curve now represents a spin-degenerate level that reduces the shell structure to a simple superposition of doubly degenerate (due to spin) states. Because the ratio between the sides of the rectangle is incommensurable, accidental degeneracies of states are absent from this spectrum. However careful observation of the energy spectrum shows several interesting features such as a convergence between the (0,0,2) and the (1,0,0) states, and several anticrossings at high-gate biases, i.e., at $V_{\text{back}}=0.958$ V between the fourth and fifth levels and at $V_{\text{back}}=0.961$ V between the third and the fourth, and the fifth and the sixth levels. The former effect is due to the presence of openings in the large metal pads along the longer gate axis which makes the variation of the (1,0,0) state more rapid than the variation of the (0,0,2) state, with the back gate potential. As a result of the different confinement, these levels would cross on the Fermi level when the lower (0,0,2) state is being filled with electrons. However, this level crossing is not possible if (0,0,2) is only partially filled with one electron because that would imply that the (1,0,0) state would immediately accept two electrons, which is prohibited by Coulomb interaction. Therefore, because of Coulomb repulsion between carriers, the two levels are constrained to remain on the Fermi level and appear to be almost degenerate. We call this configuration ''Coulomb degeneracy.'' It is to be noted that our model does not provide a complete degeneracy as the two levels are still separated at the Fermi level by a few hundredths of a meV during the charging of the (1,0,0) level. A situation similar to this ''Coulomb degeneracy'' is encountered in atomic physics when two outer orbitals with different parities are degenerate: the energetically favorable configuration for two electrons is the configuration with one electron on each orbital of parallel spin because it minimizes the Coulomb repulsion between the two particles and maximizes the exchange interaction.[21] In the present context the same reasoning would lead to one electron in each of the (1,0,0) and (0,0,2) states with parallel spins, which also minimizes Coulomb repulsion and maximizes exchange interaction. This could be accomplished by imposing the partial occupation of the (1,0,0) state subsequent to the partial occupation of the (0,0,2) state. However this subtle behavior cannot be described within the LDA wherein the exchange-correlation energy is only a function of the electron density, but not of their individual spin. This task will be addressed in our future work.[20]

There are additional interesting features in the spectrum of the quad-gate dot. Since the filling of the (0,0,2) and the (1,0,0) states proceeds sequentially, the variation of the upper levels are delineated into two distinct patterns: the energy levels characterized by the quantum number $n_x=0$, i.e., the fifth and seventh levels, now follow the variation of the lowest three levels [the (0,0,2) state in particular] with the same quantum number $n_x=0$, while the sixth level [i.e., the (1,0,1) state] with the quantum number $n_x=1$ follows the variation of the fourth level [i.e., the (1,0,0) state]. This leads to anticrossings seen at $V_{\text{back}}\cong 0.958$ and 0.961 V.

Figure 8 shows the variation with V_{back} of the potential profile along the z axis which corresponds to the longer side of the rectangle. By comparison with Fig. 5 for the square gate, it is seen that the shell ''bunching'' effect has now disappeared, but the profiles for the fifth, sixth, seventh, and eighth electrons appear to be bunched due to Coulomb degeneracy. This effect is also evident for $0.954 \leqslant V_{\text{back}} \leqslant 0.959$ V in Fig. 9 which shows the Coulomb staircase as a function of V_{back}. Aside from the regular series of long and short steps reflecting the successive charging of separated and doubly degenerate states, the Coulomb staircase shows a grouping of steps with identical widths for $N=5$, 6, and 7 electrons.

The change in the Fermi level in the dot $\Delta\mu$ upon the addition of an electron to the dot containing N electrons is the *addition energy* given by $e^2/C_s(N)=\mu(N+1)-\mu(N)$, where $C_s(N)$ is the self-capacitance of the dot. Since the dot is not in diffusive contact with the outside environment, the

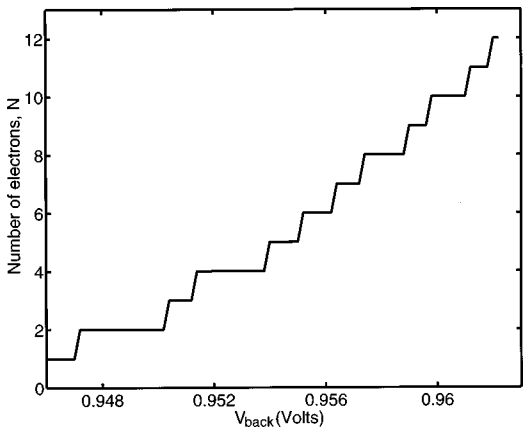

FIG. 9. Coulomb staircase for the quad-gate quantum dot; the top gates are fixed at -1.9 V.

Fermi level in the dot is not fixed, and consequently $\mu(N)$ is evaluated as the difference between the Fermi level in the 2D leads and the minimum of the bare potential energy in the dot. Figure 10(a) shows the variation of addition energy as a function of N in the square-gate dot. Each peak indicates the filling of a shell and corresponds to the wide steps in the Coulomb staircase of Fig. 6. Between the peaks, the addition energy remains small with the overall decreasing trend at high V_{back}. However, two additional peaks at $N=10$ and 16 appear in the diagram, which indeed correspond to wider steps within the orbital grouping in the Coulomb staircase. These anomalously large addition energies are caused by the splitting of the degenerate (1,0,1) from the (2,0,0)-(0,0,2) pair (at $N=10$) and the (2,0,1)-(1,0,2) pair from the (0,0,3)-(3,0,0) pair (at $N=16$), due to the anharmonicity in the confining potential induced by the many-body interaction, as mentioned before. Indeed a detailed analysis shows that the (1,0,1) state is higher in energy than the (2,0,0)-(0,0,2) pair bearing the tenth electron. Similarly, the (2,0,1)-(1,0,2) pair is higher in energy than the (0,0,3)-(3,0,0) pair which bear the sixteenth electron. These general features in the addition energy spectrum, e.g., high peaks for the shell filling and the $N=16$ peak, have indeed been observed by Tarucha *et al.*, although in a vertical quantum dot with a circular cross section.[7] It is worth mentioning that the experimental data show more peaks than the theory because of spin effects and Hund's rule in shell filling. At this stage, our model cannot account for these effects because the present LDA does not distinguish between individual spin states in the calculation of the exchange-correlation energy as mentioned before. Let us also mention that the experimental data for the circular geometry show a minimum instead of a peak at $N=10$ in the addition energy diagram, which may be due to spin effects offsetting the influence of anharmonicity in the potential.

In addition to the self capacitance, a gate-dot capacitance $C_g(N)$ may also be defined as $C_g(N)=\Delta Q/\Delta V = e/[V_{\text{back}}(N+1)-V_{\text{back}}(N)]$. In fact, C_g is just the reciprocal of the voltage step in the Coulomb staircase aside from the scaling factor e. The shell splitting at $N=10$ and 16 is also evident as a dip in C_g.

Figure 10(b) shows the variation of the addition energy as a function of N for the quad-gate dot. The lifting of the degeneracy between single-particle levels by the rectangular symmetry of the dot is apparent in the peaking of addition

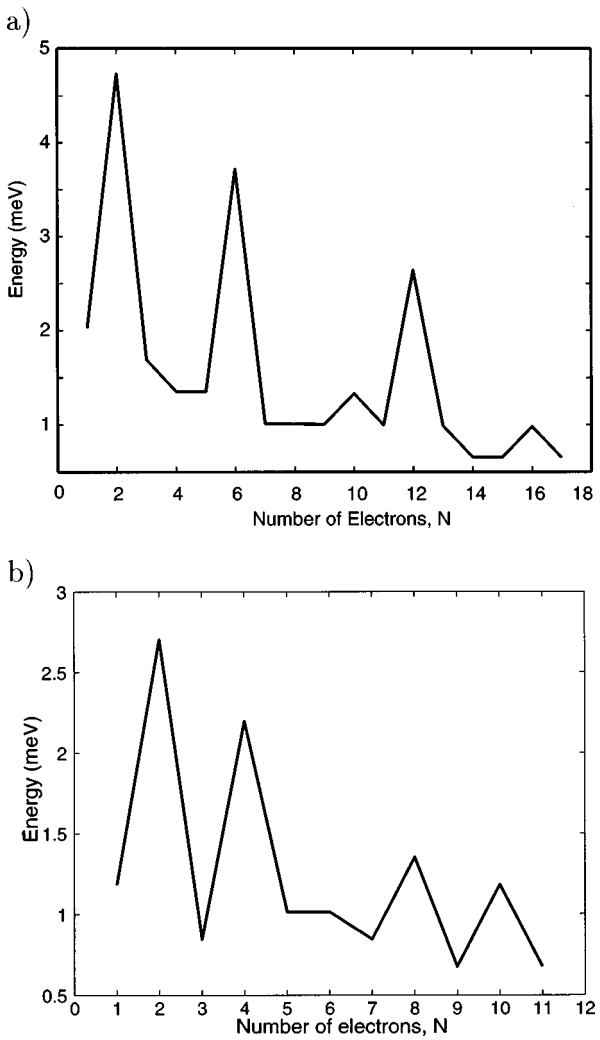

FIG. 10. Addition energy as a function of the electron number N in (a) the square-gate dot. The peaks correspond to the additional energy required to add an electron to another level in the dot. (b) The quad-gate dot. The Coulomb degeneracy effect is seen as a low charging energy at $N=6$.

energy peaks, but of decreasing amplitude, for $N=2$, 4, and 8. The Coulomb degeneracy effect is seen in the lower addition energies for $N=5$, 6, and 7.

VI. CONCLUSIONS

We have investigated the effect of the confining potential symmetry and the electron-electron interaction on the electronic properties of two quantum-dot configurations in the quantized regime. We have confirmed the formation of shell structure in highly symmetric dots which is in good agreement with experimental data. In addition, we have been able to provide deep physical insight into the shell structure and specifically, the ''bunching'' of the self-consistent electrostatic potential profile during the charging of the dot corresponding to the filling of a shell. Our analysis has also been able to investigate fine physical details such as anomalously large addition energies at $N=10$ and 16 which are due to lifting of degeneracies in the third and fourth shells caused by anharmonicity in the potential. In asymmetric quantum dots, the shell structure vanishes but under particular con-

finement we have shown that electron-electron interaction leads an anomalous shell caused by Coulomb degeneracy—a merging of two energy levels caused by electron repulsion during the charging of the dot which has its analogy in atomic physics.

ACKNOWLEDGMENTS

We would like to thank L. Fonseca, I.-H. Lee, P. von Allmen, S. Tarucha, and H. Tamura for valuable discussions, and K. Hess for providing a copy of his work prior to publication. This work was supported by NSF Grant No. NSF-ECS 95-09751 and ARO Grant No. DAAH04-95-0190.

APPENDIX

Here we give the expressions for the exchange and correlation potential[6] $\mu_{xc}(n)$ that we have used in the Hamiltonian:

$$\mu_{xc}(n)=\frac{d}{dn}\,[n\epsilon_{xc}(n)], \tag{A1}$$

where $\epsilon_{xc}(n)$ is the sum of the exchange $\epsilon_{ex}(n)$ and correlation $\epsilon_{corr}(n)$ energies per electron, derived from LDA i.e., $\epsilon_{xc}(n)=\epsilon_{ex}(n)+\epsilon_{corr}(n)$

$$\epsilon_x(n)=\frac{-0.4582}{r_s}, \tag{A2}$$

r_s is expressed in terms of the effective Bohr radius in GaAs, $a_0^*=\epsilon_r a_0/m^*$ [here ϵ_r is the dielectric constant of GaAs ($=13.2$) and m^*, the effective mass of electron in GaAs ($=0.067m_0$)] and the local electron concentration, $n(r)$ as

$$r_s=\left[\frac{3}{4\pi n(r)}\right]^{1/3}\frac{1}{a_0^*}. \tag{A3}$$

The correlation energy, however, is dependent on whether we are in the high ($r_s\ll 1$) or low ($r_s\gg 1$) density regime. The correlation energy is parametrized as[16]

$$\epsilon_{corr}=\frac{B}{1+C\sqrt{r_s}+Dr_s}\quad (r_s\geqslant 1),$$

$$\epsilon_{corr}=E+F\,\ln r_s+Gr_s+Hr_s\,\ln r_s\quad (r_s<1),$$

$$B=-0.1423,\quad C=1.0529,\quad D=0.3334,$$

$$E=-0.0480,\quad F=0.0311,\quad G=-0.0116,\quad H=0.0020.$$

The energies and potentials are expressed in scaled atomic units, i.e., $2R_y^*=2R_y m^*/(m_0\epsilon_r^2)$. The exchange correlation potential μ_{xc}, which is given by Eq. (A1), turns out to be

$$\mu_{xc}=\mu_{ex}+\mu_{corr},$$

$$\mu_{ex}=-\frac{0.611}{r_s},$$

$$\mu_{corr}=\epsilon_{corr}+\frac{r_s}{3}\frac{B\left[\dfrac{C}{2\sqrt{r_s}}+D\right]}{[1+C\sqrt{r_s}+Dr_s]^2}\quad (r_s\geqslant 1),$$

$$\mu_{corr}=\epsilon_{corr}-\frac{r_s}{3}\frac{F}{r_s}+G+H(1+\ln r_S)\quad (r_s<1).$$

[1] H. van Houten, C. W. J. Beenakker, and A. A. M. Staring, in *Single Charge Tunneling*, edited by H. Grabert and M. H. Devoret (Plenum, New York, 1992).
[2] D. V. Averin, A. N. Korotkov, and K. K. Likharev, Phys. Rev. B **44**, 6199 (1991).
[3] U. Meirav and E. B. Foxman, Semicond. Sci. Technol. **10**, 255 (1995).
[4] D. Leonard, K. Pond, and P. M. Petroff, Phys. Rev. B **50**, 11 687 (1994).
[5] N. N. Ledenstov *et al.*, Phys. Rev. B **54**, 8743 (1996).
[6] J. Haug, R. H. Blick, and T. Schmidt, Physica B **212**, 207 (1995).
[7] S. Tarucha, D. G. Austing, T. Honda, R. J. van der Hage, and L. P. Kouwenhoven, Phys. Rev. Lett. **77**, 3613 (1996).
[8] D. Jovanovic and J. P. Leburton, Phys. Rev. B **49**, 7474 (1994).
[9] M. Stopa, Phys. Rev. B **48**, 18 340 (1993).
[10] D. V. Averin and K. K. Likharev, in *Mesoscopic Phenomena in Solids*, edited by B. L. Altshuler, P. A. Lee, and R. A. Webb (Elsevier, Amsterdam, 1990).
[11] M. Macucci, K. Hess, and G. J. Iafrate, Phys. Rev. B **55**, R4879 (1997).
[12] U. Meirav, M. A. Kastner, and S. J. Wind, Phys. Rev. Lett. **65**, 771 (1990).
[13] M. A. Kastner, Rev. Mod. Phys. **64**, 849 (1992).
[14] A. Kumar, S. E. Laux, and F. Stern, Phys. Rev. B **42**, 5166 (1990).
[15] M. Macucci, K. Hess, and G. J. Iafrate, Phys. Rev. B **48**, 17 354 (1993).
[16] J. P. Perdew and Alex Zunger, Phys. Rev. B **23**, 5048 (1981).
[17] R. Kosloff and H. Tal-Ezer, Chem. Phys. Lett. **127**, 223 (1986).
[18] M. Stopa, Phys. Rev. B **54**, 13 767 (1996).
[19] R. O. Jones and O. Gunnarsson, Rev. Mod. Phys. **61**, 689 (1989).
[20] S. Nagaraja and J. P. Leburton (unpublished).
[21] J. C. Slater, *Quantum Theory of Molecules and Solids* (McGraw-Hill, New York, 1963).